Analytica Chimica Acta 1148 (2021) 238169

Contents lists available at ScienceDirect

Analytica Chimica Acta

journal homepage: www.elsevier.com/locate/aca

Photoinduced-electron transfer coupled with DNA cross-chain displacement multiple amplification for fluorescence biosensing of MicroRNA

Qianqian Cai [1], Hongkun Li [1], Wei Cao, Guifen Jie*

Key Laboratory of Optic-electric Sensing and Analytical Chemistry for Life Science, MOE, Shandong Key Laboratory of Biochemical Analysis, Key Laboratory of Analytical Chemistry for Life Science in Universities of Shandong, College of Chemistry and Molecular Engineering, Qingdao University of Science and Technology, Qingdao, 266042, PR China

HIGHLIGHTS

- A new fluorescence biosensor based on photoinduced-electron transfer of AgNCs/DNA and G-quadruplex was developed.
- The fluorescence biosensor was designed by using unique DNA cross-chain displacement cyclic amplification strategy.
- The new fluorescent AgNCs/DNA probe was synthesized based on high affinity of Ag to cytosine (C) rich ssDNA.
- The guanine rich ssDNA was used to synthesize G-quadruplexes quencher in PET process.

GRAPHICAL ABSTRACT

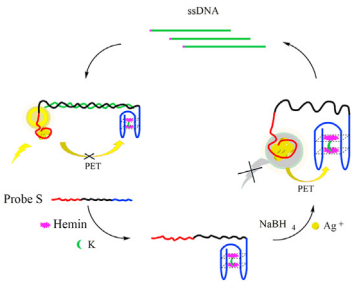

ARTICLE INFO

Article history:
Received 28 August 2020
Received in revised form
20 December 2020
Accepted 21 December 2020
Available online 6 January 2021

Keywords:
Fluorescence biosensor
Photoinduced-electron transfer
Cyclic amplification
AgNCs/DNA
G-quadruplex complex

ABSTRACT

In this work, a new fluorescence biosensor platform based on distance-dependent photoinduced-electron transfer (PET) coupled with target cross-chain displacement cyclic amplification strategy was developed to detect MicroRNA. The DNA cross structure was cleverly designed to protect restriction site, then multiple amplification reactions of target cycle and chain replacement based on DNA cross-configuration were carried out in the presence of primer, polymerase and cutting enzyme, thus a large number of single-stranded (ss) DNA products (S1 and S2) can be exported by inputting a small amount of target miRNA. The fluorescent AgNCs/DNA probe was synthesized based on high affinity of Ag to cytosine (C) rich in ssDNA acting as electron donor, and guanine (G) rich ssDNA can form G-quadruplex complex acting as electron receptor to induce PET process. S1 and S2 hybridized with flexible single-stranded DNA COM 1 and Com 2, forming rigid double-stranded DNA to inhibit fluorescence quenching PET process, so the corresponding fluorescence was recovered. Thus the miRNA-induced amplified products can specifically result in fluorescence changes by PET, and the changes increase with increasing miRNA concentration. Therefore, the proposed fluorescent biosensor can be applied to quantitative determination of miRNA-182-5p, which has great potential in early clinical diagnosis of miRNAs related diseases.

* Corresponding author.
E-mail address: guifenjie@126.com (Guifen Jie).
[1] These two authors contributed equally to this work.

https://doi.org/10.1016/j.aca.2020.12.044
0003-2670/

1. Introduction

In recent years, the death rate from cancer is getting higher. Therefore, exploring new cancer prevention and treatment methods have become a priority [1]. It is well known that the specific expression of DNA or MicroRNA (miRNA) is closely related to the occurrence and development of tumors [2]. Non-coding small fragments of single-stranded RNA molecules (miRNAs) are a class of endogenous, 20 to 24 oligonucleotides. They show important regulatory roles in a series of biological processes, including early development, cell proliferation, apoptosis, cell death, fat metabolism, and cell differentiation [3]. In addition, many studies have shown that the abnormal expression of miRNAs is related to a variety of human diseases, such as cancer, malignant tumors, cardiovascular and cerebrovascular diseases, and neurodegeneration [4–7]. Therefore, ultra-sensitive and selective detection of various nucleic acid-related cancers are significant in biological research, forensic evidence and early cancer screening. It is reported that miR-182 is overexpressed in prostate cancer tissues and has been identified as an oncogene, so accurate, rapid, and cost-effective quantification of miR-182-5p is vital for its application in clinical treatment [8].

However, it is possible that miRNA content may appear in very small amounts during research and diagnosis. Therefore, various circular amplification strategies must be used to determine trace levels of specific sequences [9]. At present, target circular amplification strategy combines different DNA structures, such as hairpin DNA [10], Y-linked DNA [11], DNA pliers [12] etc, which are beneficial to improve detection sensitivity of trace level target for biosensors. However, a large amount of DNA strands generated by these cyclic processes are wasted, resulting in low efficiency and high cost of target detection. Therefore, DNA structure needs to be reasonably designed to achieve target recycle amplification, avoid excessive waste, and improve the analysis performance to meet the development needs of biological research and clinical diagnosis. The regeneration strategy has the advantages of multiple reuses, saving material resources, and reducing experimental costs. It has been widely used in biological materials, chemical absorption, medicine and other fields. In recent years, several traditional miRNAs detection methods based on real-time polymerase chain reaction, Northern hybridization, microarray, bioluminescence, electroluminescence, and electrochemistry, have been developed [13–15]. Especially, fluorescence technology is considered to be a promising detection method due to the advantages of simplicity, rapid analysis, low cost and high sensitivity [16].

This study is to design a fluorescent biosensing platform for detecting miRNA-182-5P based on distance-dependent light-induced electron transfer combined with DNA displacement and target recycle multiple amplification. Through DNA cross-chain design, a single target miRNA input can be converted into a large amount of ssDNA (S1 and S2) output. A fluorescent detection probe is uniquely designed, which includes a C-rich DNA sequence as synthetic template of Ag nanoclusters (AgNCs), a DNA sequence complementary (Com) with the amplification products (S1 and S2), and a G-base-rich sequence forming G-tetramer/hemin, so the distance-dependent photoinduced electron transfer (PET) from DNA/AgNCs (electron donor) to G-tetramer/heme complex (electron acceptor) can be controlled by target. In the presence of target-amplification products (ssDNA), the initial flexible single-stranded complementary sequence (COM) in probe changes to rigid double-stranded DNA, the distance between electron donor and acceptor becomes longer to block PET, so the quenched fluorescence of DNA/AgNCs restores. Thus, a fluorescence biosensor based on signal change of DNA/AgNCs can be developed for the detection of target miR-182-5p assay. It is important that the nucleic acid products obtained by circular amplification can be fully utilized, which avoids waste and saves experimental costs at a certain extent.

2. Experimental section (materials and apparatus see supporting information)

2.1. Preparation of solution

Sodium borohydride solution (0.001 M) is prepared. 0.0379 g of $NaBH_4$ was added to 1000 mL of ultrapure water at lower temperature.

Preparation of hemin solution (0.001 M). 0.066 g of Hemin was dissolved in 100 mL of DMSO, heating at 37 °C in water bath, and stored at 4 °C in dark.

2.2. Preparation of DNA/AgNCs [17]

In a 100 μL reaction system containing 78 μL of phosphate buffer solution (PBS, pH = 7.4, 20 mM), 6.0 μL of 1 mM $AgNO_3$ solution and Probe S (1×10^{-4} M) were added. After reacting for 1 h at room temperature, 6.0 μL 1 mM of $NaBH_4$ solution was added and incubated at 4 °C for 6 h under dark conditions. After reaction was completed, it was placed in a clean brown glass bottle and stored at 4 °C until use.

2.3. Fluorescence reaction system

Target recycle amplification process based on DNA cross-chain displacement is performed. First, 5.0 μL of longer single-stranded DNA H1 and H2 were annealed at 90 °C for 5 min, respectively, then slowly cooled to room temperature, and stored at 4 °C for use. In a 20 μL reaction system containing 2.0 μL of H1 (10 μM), 2.0 μL of H2 (10 μM), 2.0 μL of Primer1 (10 μM), 2.0 μL of Primer2 (10 μM), and 2.0 μL of target at different concentrations (microRNA-182-5p), 1.0 μL of dNTPs (0.5 mM) was added. In the reaction system, 8.0 U of nicking endonuclease (Nt.BbvCI), 2.0 U of Klenow fragment (2.0 U) were added to the CutSmart buffer solution and NEBuffer 2 solution, reacting at 37 °C in constant temperature shaker for 2 h. Then the reaction was stopped at 80 °C for 20 min. Finally, single-stranded S1 and S2 are obtained. Then, in 100 μL detection system containing 8.0 μL of PB solution, 5.0 μL of Probe S1 (1×10^{-4} M), 5.0 μL of Probe S2 (1×10^{-4} M), 10 μL of 1.0×10^{-4} M Hemin, and 50 μL of KNO_3 (1.0 M) were added and reacted at room temperature for 2 h, then 6.0 μL of 0.001 M $AgNO_3$ solution was added to continue the reaction at room temperature for 1 h. Next, 6.0 μL of freshly prepared $NaBH_4$ was added and incubated at 4 °C in dark for 6 h. Finally, 10 μL of the amplification reaction products were added and reacted at room temperature for 2 h. The fluorescence signal of the reaction system is then detected.

2.4. Design principle of the signal probe

Due to the high affinity of Ag^+ to cytosine, single-stranded DNA sequences rich in cytosine (C) are commonly used to synthesize fluorescent DNA/AgNCs. In this work, a new nucleic acid probe (Probe S, Scheme 1) with three-segment DNA was designed, including C-base-rich DNA (C, red region) as template for AgNCs synthesis, DNA sequence complementary with ssDNA produced by amplification reaction (Com, black region), G-base-rich DNA (G, blue region) forming G-tetramer/Hemin complex. The potassium ion (K^+) and hemin (Hemin) induced formation of G-tetramer/hemin complex (electron acceptor) and fluorescent DNA/AgNCs (electron donor) were synthesized by introducing $AgNO_3$ and $NaBH_4$ to the solution. In this case, Com segment is a flexible single

strand DNA, which results in light-induced electron transfer (PET) from electron donors (AgNCs) to electron acceptors (G-quadruplex/heme) due to short distance between them, so the fluorescence quenching efficiency is relatively high. When the amplification product (ssDNA) is added, ssDNA can hybridize with COM fragment (black region) to form rigid dsDNA through conformational transformation, the distance between electron donor (AgNCs) and electron acceptor (G-quadruplex/heme) increases, so the photoelectron transfer (PET) process is hindered, and the fluorescence of AgNCs is restored.

3. Results and discussion

3.1. Characterization of DNA/AgNCs

Fig. 1A is transmission electron microscopy (TEM) image of the fluorescent DNA/AgNCs. Ag^+ is in situ reduced to AgNCs on the C-rich sequence by $NaBH_4$, which is evenly distributed. The morphology and particle size of AgNCs are relatively uniform, and the average particle size is 2 nm, which is consistent with definition of nanoclusters (d < 2 nm) [18]. Fig. 1B is fluorescence emission spectrum of DNA/AgNCs, showing a narrow and symmetrical fluorescence emission peak at 560 nm. Fig. 1C is UV−vis absorption spectra of DNA/AgNCs, a feature strong peak of Ag nanoclusters is at 428 nm, indicating the successful synthesis of Ag NCs [19]. In addition, the characteristic peak of DNA is at 260 nm, which proved that the DNA/AgNCs were successfully prepared.

3.2. Principle of MicroRNA Detection Based on Distance-dependent photoinduced electron transfer coupled with cross-chain displacement and target cyclic amplification

This work aims to design a fluorescence biosensing platform based on distance-dependent photoinduced electron transfer coupled with cross-chain displacement and target cyclic amplification for MicroRNA detection (Scheme 2). Hairpin H1 and H2 are firstly annealed together, then reacte for 2 h to form DNA cross-configuration. After target miRNA is added, it hybridizes with H2 and the exposed fragment of H1 reacts with Primer1. With the action of Klenow fragment DNA polymerase and dNTPs, Primer 1 can be expanded with H1 as a template until it is completely complementary to H1, forming dsDNA 1 with Nt.BbvCI restriction site and replaces the hybrid chain H2-target. Then, dsDNA 1 is cut by Nt.BbvCI nicking enzyme to produce vast product chain S1.

At this time, the hybrid portion of target-H2 is separated from the original cross configuration, and the exposed single-stranded fragment can also be complementary to Primer2. In the presence of dNTPs and Klenow polymerase, Primer2 runs along H2 and extend until it is completely complementary to H2 to form dsDNA 2, while target miRNA is replaced into next cycle. The formed dsDNA 2 also has Nt.BbvCI cleavage site, and the cutting dsDNA 2

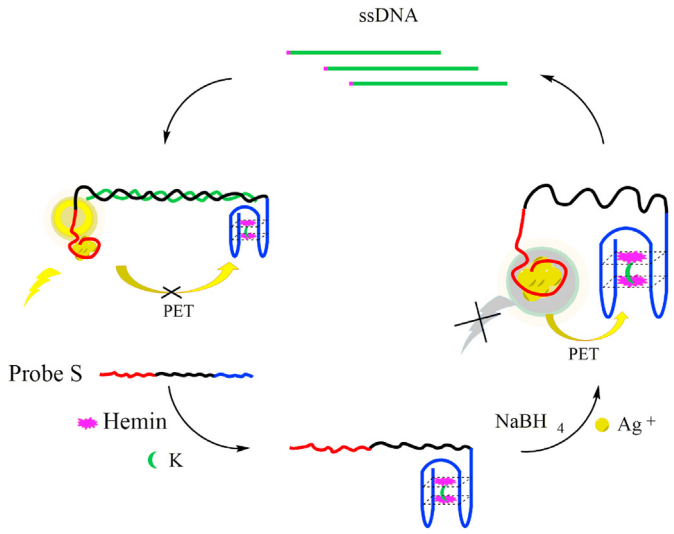

Scheme 1. Design principle of probe.

can also polymerize to result in accumulation of single-chain S2. Through such cycling amplification, single target miRNA can be converted into a large amount of output ssDNA, which significantly enhances the sensitivity of miRNA detection. Probe1 and Probe 2 with C-base-rich fragments capture Ag^+ and was in situ reduced to AgNCs by $NaBH_4$, and G-base-rich DNA form G-quadruplex/heme complex in the presence of Hemin and KNO_3. Since the flexible single-stranded COM region cannot be supported, the electron donor (AgNCs) and electron acceptor (G-quadruplex/Hemin) undergo light-induced electron transfer reactions at close range, resulting in fluorescence quenching of AgNCs. After the cycling amplification products (S1and S2) hybridize with COM region of the probe, forming rigid double-stranded DNA to increase the distance between G-quadruplex/hemin) and AgNCs. As a result, the light-induced electron transfer reaction is hindered, and the fluorescent signal of AgNCs is restored.

3.3. Gel electrophoresis characterization of cyclic amplification strategy based on target cross-chain displacement

Polyacrylamide gel electrophoresis was used to analyze the cyclic amplification strategy of target cross-chain displacement. As shown in Fig. 2, lanes A and B are single-chain H1 and single-chain H2, respectively. Lane C contains H1 and H2 at the same concentration, they hybridized with each other to form cross-chain structure, so H1 and H2 bands are weaker than those in lanes A and B, and a band with larger molecular weight appears in lane 3, indicating the hybridization of H1 and H2 is successful. Lane D is

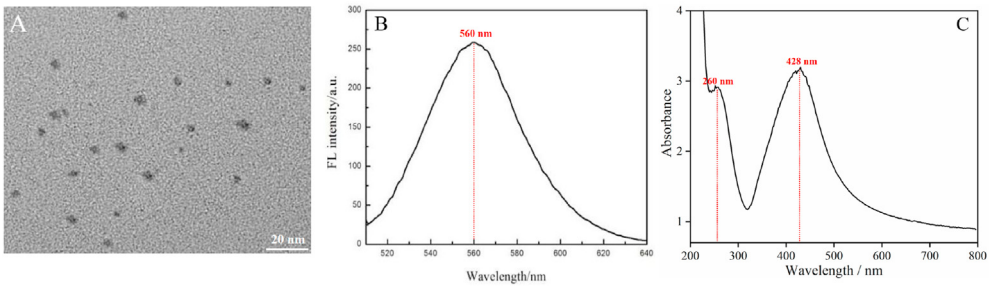

Fig. 1. (A) TEM image of DNA/AgNCs, (B) Fluorescence spectrum of DNA/AgNCs. (C) UV−vis absorption spectrum of DNA/AgNCs.

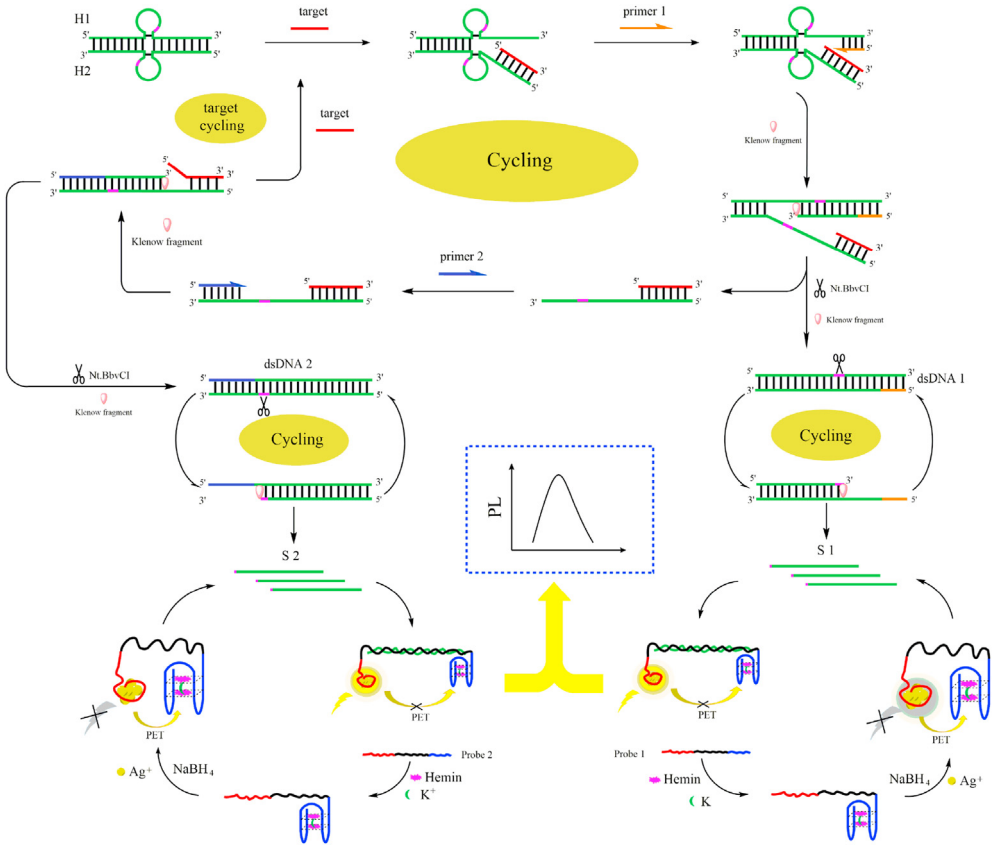

Scheme 2. Principle of MicroRNA detection based on distance-dependent photoinduced electron transfer coupled with cross-chain displacement and target cyclic amplification.

the mixture of H1+H2+Target, and distinct new band appears, indicating that target hybrids with H2 successfully. Lane E is the mixture of H1+H2+Target + Primer1+Primer2, a new Primer band at lower position was observed, but no product bands are produced in the absence of the enzyme. When Klenow fragment DNA polymerase and Nt.BbvCI nicking endonuclease were further added, two product chains (S1, S2) are obtained at the bottom in line F, indicating that the cycle reaction has been successfully performed and generated ssDNA.

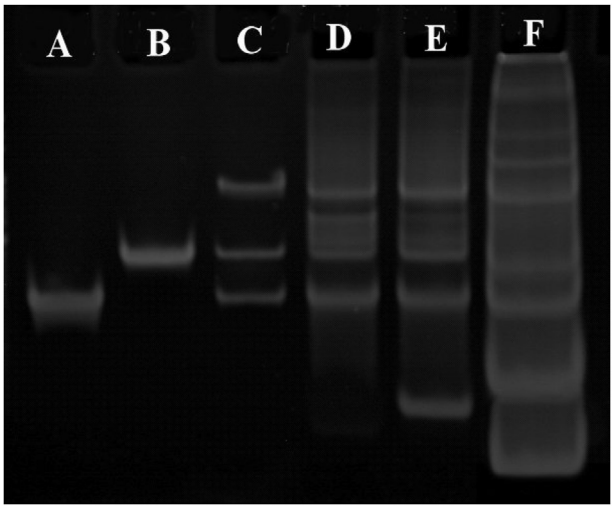

Fig. 2. Gel electrophoresis analysis of the target-induced DNA-cross configuration strand displacement cycling amplification process. A: 10 μL 1.0 × 10^{-6} M H1, B: 10 μL 1.0 × 10^{-6} M H2, C: the same concentration of H1+H2, D: mixture of H1+H2+Target, E: mixture of H1+H2+Target + Primer1+Primer2 without enzyme, F: mixture of H1+H2+Target + Primer1+Primer2 with enzyme.

3.4. Feasibility study of the fluorescence biosensing platform

In order to verify the feasibility of the fluorescence biosensing platform, the performance of the fluorescence probes were firstly explored. The probe contains a base C-rich fragment, a base G-rich fragment, and a complementary fragment COM. Using cytosine-rich single-stranded DNA (5′-CCCCACCCCACCCCA-3′, named C) as a template and $NaBH_4$ as a reducing agent, DNA/AgNCs with obvious fluorescence signals were successfully synthesized (Fig. 3A, curve c). Conversely, under the same conditions, when G-rich DNA and COM fragment are selected as template, the DNA/AgNCs cannot be obtained, so fluorescence signal is low (curves a, d). In addition, the designed probes (including C, COM and G parts) were used as templates to prepare DNA/AgNCs, the fluorescence signal is higher than that of C, as the purine sequence (G) can greatly enhance the fluorescence signal of DNA/AgNCs synthesized with cytosine-rich sequences (curve b).

In order to further study the feasibility of the fluorescence biosensor, two comparative experiments were performed. Single-stranded DNA complementary with COM region in probe could not be generated without target, so light-induced electron transfer between AgNCs and G-quadruplex/heme cannot be prevented, the fluorescence signal is low (Fig. 3B, curve a). In the presence of target, the resulting single-stranded DNA hybridized with COM to form rigid double-stranded DNA, which effectively prevented electron transfer, leading to fluorescence recovery (Fig. 3B, curve b). These results prove that the fluorescence biosensor has good

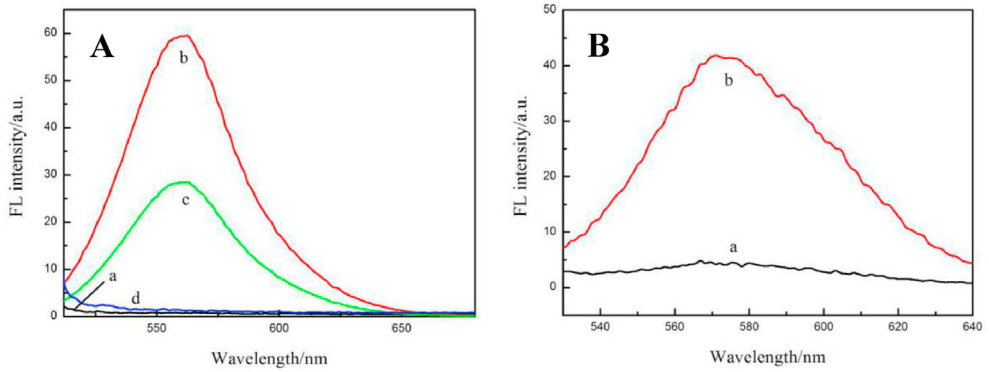

Fig. 3. (A) Fluorescence emission spectra of DNA/AgNCs obtained using some fragments of ProbeS. (a) Rich-G, (b) ProbeS, (c) rich-C, (d) COM, (B) Fluorescence emission spectra of ProbeS (a) in the absence of target, (b) in presence of target (0.5 nM).

feasibility for target assay.

3.5. Fluorescence of DNA/AgNCs/probes under different conditions

In the presence of K^+ and Hemin, guanine (G)-rich single-stranded DNA sequence can be folded into G-quadruplex structure, and then G-quadruplex/hemin complex is formed. DNA/AgNCs in ProbeS generated strong fluorescence signal (Fig. 4, curve a), and the signal did not change significantly when only K^+ was added (Fig. 4, curve b). However, when K^+ and hemin were present simultaneously, the signal of DNA/AgNCs decreased significantly (Fig. 4, curve c), indicating that only the preformed G-quadruplex/hemin complex can cause fluorescence quenching, which may be related to the shortened distance between hemin and DNA/AgNCs. When the amplification product (ssDNA) was added, the fluorescence signal increased, indicating that the distance between hemin and DNA/AgNCs increase after ssDNA hybridized with COM region in probe to form rigid dsDNA.

3.6. Optimization of experimental conditions

In order to apply this fluorescence biosensing platform for miRNA assay and obtain best detection results, the experimental conditions were optimized. The incubation time and temperature are critical for efficient hybridization of nucleic acid sequences, thus they are optimized. The temperature optimization experiments for nucleic acid hybridization were performed (Figure S1A), and it was clear that the highest hybridization efficiency is at 37 °C by FL signal comparison, indicating that the optimized temperature is 37 °C.

Moreover, the incubation time for nucleic acid hybridization at 37 °C was optimized, the fluorescence signal gradually increases with the increase of incubation time, and the FL signal is no longer changes until 2 h, so the best hybridization time is 2 h.

As we all know, the salt concentration is important for nucleic acid hybridization, so we mainly optimized the concentration of PB solution and K^+ in Figure S1C and Figure S1 D. It is found that when the concentration of salt ion was very low, nucleic acid hybridization efficiency was bad, so the fluorescence recovery signal was small. With the increasing of salt ion concentration, the nucleic acid hybridization rate increased, and the fluorescence recovery signal was enhanced until saturation, so the optimized concentration of PB solution and K^+ for nucleic acid hybridization are 20 mM and 0.5 M.

The synthesized DNA/Ag NCs is essential to fluorescence signal, so a series of optimizations were performed. As shown in Figure S2A, the concentration of $AgNO_3$ was first optimized, the FL signal gradually increases and does not change after 1 mM, indicating that 1 mM $AgNO_3$ is the saturation concentration for C-base rich DNA. In addition, the incubation temperature of C-base rich DNA and $AgNO_3$ was also optimized, as sodium borohydride is more stable at low temperature, so the best temperature is 4 °C.

The pH of phosphate buffer solution can directly affect the activity of DNA and enzymes, thus affecting the change of fluorescence signal. As shown in Figure S3, the fluorescence intensity of the solution decreases with increasing pH, while the relative value of fluorescence intensity increases with increasing pH, suggesting the fluorescence recovery efficiency increases with increasing pH. At the same time, when the pH value is higher than 7.4, the fluorescence intensity is too weak, which is not suitable for high sensitive detection of the fluorescence biosensor. Therefore, when a relatively neutral pH of 7.4 is chosen, the fluorescence intensity and recovery are relatively high, so the optimal buffer pH is 7.4.

The concentration of hemin is important for the formation of G-tetramer/heme complex (electron acceptor), which in turn affects the efficiency of PET and FL signal. So hemin concentration in the absence and presence of target is optimized (Figure S4A). The relationship between fluorescence recovery efficiency and hemin concentration were also studied. With the increase of hemin concentration, the fluorescence recovery efficiency firstly increases and

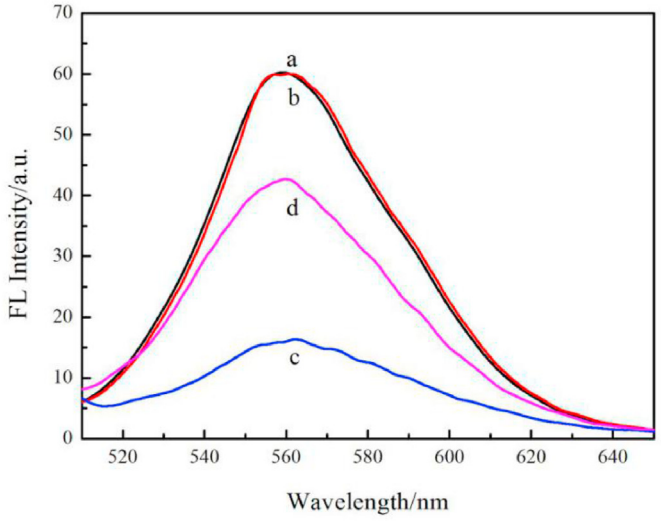

Fig. 4. Fluorescence emission spectra of DNA/AgNCs/ProbeS under different conditions. (a) ProbeS, (b) ProbeS + K^+, (c) ProbeS + Hemin + K^+, (d) ProbeS + Hemin + K^+ + cycling products. The fluorescence emission and excitation peaks are at 560 nm and 428 nm, respectively.

then gradually decreases, and reaches highest in 10 μM (Figure S4B), suggesting that the optimal concentration of hemin is 10 μM.

There are two other important parameters in the fluorescence sensing system, the concentration of Klenow fragment DNA polymerase and Nt.BbvCI nicking endonuclease, both of which have effects on target recycle and sensitivity of the sensing system. The optimal amount of the two enzymes were optimized by fixing one value and changing the other to study the change trend of the PL signal. As shown in Fig. 5A, the effect of polymerase on the sensing system was studied. When the concentration of Nt.BbvCI was maintained at 0.3 U/μL, the fluorescence signal increases with increasing polymerase concentration until 0.2 U/μL, then it no longer increases, suggesting that the optimal concentration of Klenow fragment DNA polymerase is 0.2 U/μL. Similarly, the concentration of Klenow fragment DNA polymerase was kept at 0.2 U/μL, the fluorescence signal increases as the concentration of nicking enzyme increases, then it will hardly change until 0.4 U/μL. Therefore, the optimal concentration of Nt.BbvCI nicking endonuclease is 0.4 U/μL.

We determine the amount of the two enzymes by controlling a single variable, and find that when the dosage of the two enzymes increase, the working efficiency per unit time would increase, and the generated fluorescence signal become larger. When the amount of the enzyme increases to a certain amount, the signal finally tend to be stable, so as to determine the optimal amount.

As for signal change trends induced by Klenow fragmen and Nt.BbvCI nicking endonuclease, the amount of amplification product chain S1 and S2 increase in the first period of time with increase of enzyme dosage, thus the amounts of rigid double chains obtained by hybridization of S1 and S2 with the corresponding complementary flexible single DNA increase, then the distance between the AgNCs as electron donor and the G4-chain-Hemin compound as electron acceptor increase, and electron transfer effect is hindered, so the fluorescence signal restore to higher value. However, the amount of S1 and S2 is ultimately determined by the amount of H1 and H2 in the hairpin chain, so the fluorescence recovery signal will reach its maximum value, and the signal will not change when the amount of enzyme increases from this time.

3.7. Relationship between fluorescence recovery efficiency and space length of DNA/AgNCs and G-tetramer/hemin

Studies have shown that photoinduced-electron transfer (PET) effect decreases with increasing distance between electron donor and electron acceptor. However, previous reports have only studied cases where the length is less than or equal to 15 bp, which is too short and cannot be applied to detection of small oligonucleotide, such as miRNAs with a length of 20–24 bp. In order to further explore the distance dependence of photoelectron induced effect, we designed a series of biological probes with different lengths (15–26 bp) of complementary fragments (COM) and target RNA (15–26 bp) correspondingly, the distance between donor and acceptor during PET process can be adjusted. Fig. 6A shows the fluorescence recovery efficiency with different space length. When the complementary region is 15 bp, the length of double-stranded DNA is about 5.2 nm, and $(F-F_0)/F_0$ is almost zero at this short distance. With increased distance, the fluorescence recovery efficiency increases and can reach more than 1 at 22 bp (about 7.5 nm), suggesting that increasing distance can inhibit the PET process at varying degrees. The results further confirmed that the distance-dependent PET mechanism is feasible for our biosensor in MicroRNA-182-5p detection. More importantly, the platform can be used for detection of longer RNA or DNA only by adjusting the length and sequence of COM.

3.8. Fluorescence biosensing platform for MicroRNA Detection Based on Distance-dependent photo-induced electron transfer coupled with target cross-chain displacement cyclic amplification

Under the optimal experimental conditions, the fluorescence biosensor was used to detect microRNA-182-5p concentration. As shown in Fig. 6B, as the concentration of target MicroRNA-182-5p increases, the fluorescence signals continues to increase, indicating that target can trigger the cycling amplification reaction, and the products can hybridize with complementary fragments (COM) to hinder the quenching reaction to AgNCs fluorescence during PET process, so the DNA/AgNCs fluorescence can recovered.

Fig. 7 shows the relationship between fluorescence signal and concentration of MicroRNA-182-5p. It can be seen that the fluorescence signal has a good linear relationship with MicroRNA-182-5p concentration in the range from 1.0 pM to 100 nM, and the detection limit is 0.6 pM. Compared with other reported methods for miRNA sensing (Table S2), our method is more sensitive for miRNA detection. Under the same experimental conditions, the fluorescence signal of 5.0 pM target was subjected to five consecutive parallel detection with the biosensor, the relative standard deviation (RSD) was calculated to be 5.1%, indicating that the fluorescence biosensing platform based on distance-dependent light-induced electron transfer and target cross-chain displacement cyclic amplification has good reproducibility for detection of MicroRNA's.

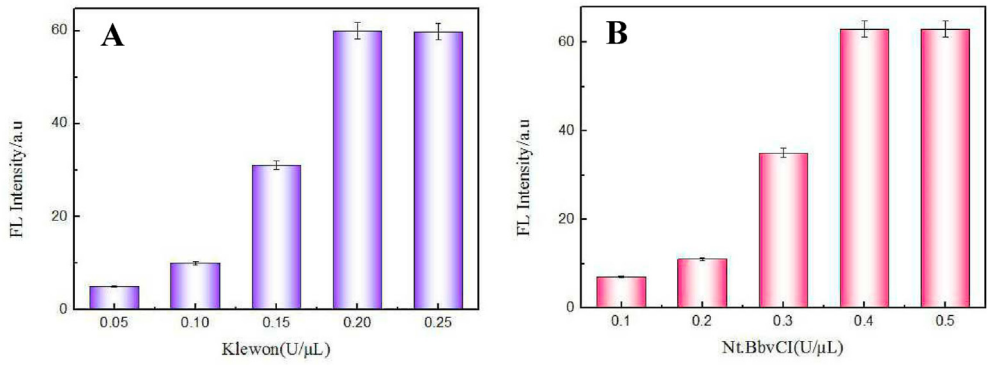

Fig. 5. Influence of enzyme concentration on fluorescence intensity. (A) Klenow fragment DNA polymerase; (B) Nt.BbvCI nicking endonuclease (error bars show mean standard deviations of three determinations).

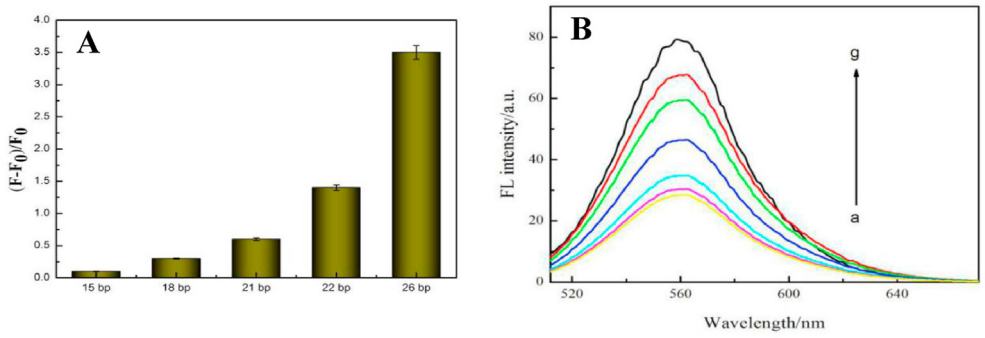

Fig. 6. (A) Relationship of fluorescence recovery efficiency and space length of DNA/AgNCs and G-quadruplex/hemin (error bars show mean standard deviations of three determinations); (B) Fluorescence responses of the biosensing platform to different microRNA-182-5p concentrations. (a) 0.0 pM, (b) 1.0 pM, (c) 10.0 pM, (d) 100 pM, (e) 1.0 nM, (f) 10.0 nM, (g)100 nM.

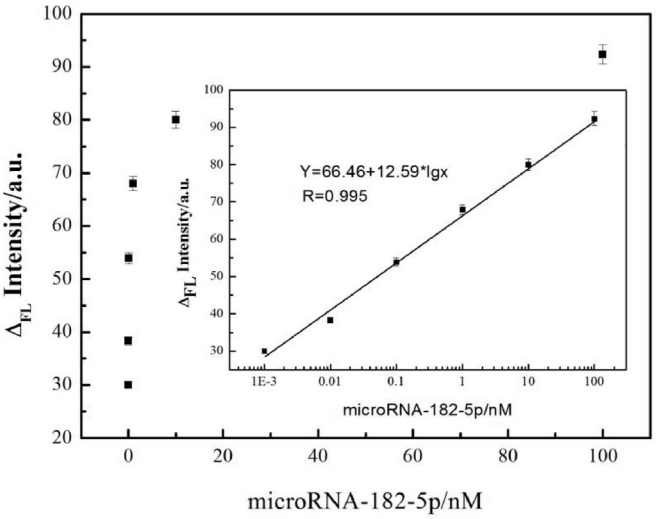

Fig. 7. The relationship between FL signal and MicroRNA-182-5p concentration (1.0 pM–100 nM). (insert: The logarithmic calibration plot for MicroRNA-182-5p detection) (error bars show mean standard deviations of three determinations).

3.9. Selectivity of fluorescent biosensor

To further explore selectivity of the fluorescence biosensor, miRNA-21, miRNA-141, and miRNA-155 were selected as interfering agents, and blank samples were used as contrasts. As shown in Fig. 8A, only target miRNA-182-5p has a distinct fluorescence signal, while miRNA-155, miRNA-141, miRNA-21 all have no obvious fluorescence signal. Whatsmore, as for the detection of every miRNA, three sets of parallel experiments (orange, purple and pink columns) were done, and these FL signals are very stable, indicating that the method has good selectivity for miRNA detection. In addition, the experiments for different isomiRs of the target microRNA were also studied (Fig. 8B). Single-base mismatched target (T1), two-base mismatched target (T2), three-base mismatched target (T3), and random sequence (R) were chosen for detection. The FL signal of target is obviously higher than those of the other mismatched targets. Compared with the signal of target (100%), the signals of single-base mismatched target, two-base mismatched target, three-base mismatched target, and random sequence reached 69.7%, 42.7%, 21.9% and 2.4%, respectively, these results demonstrated the high specificity of the FL biosensor.

3.10. Anti-interference detection

The detection of MiRNA is generally performed in complex systems, which is required to have strong anti-interference ability. Therefore, the anti-interference ability of the method in complex system is tested. In a 10 μL reaction system containing 40 ng humans lung cancer cell A549 total RNA, target miRNA-182-5p at different concentrations was detected. As can be seen from Figure S5, with the reduction of miRNA concentration (from 10 pM to 0.1 pM), the fluorescence signals decreased, and showed obvious contrast with that of blank group (0 pM). Furthermore, the signals

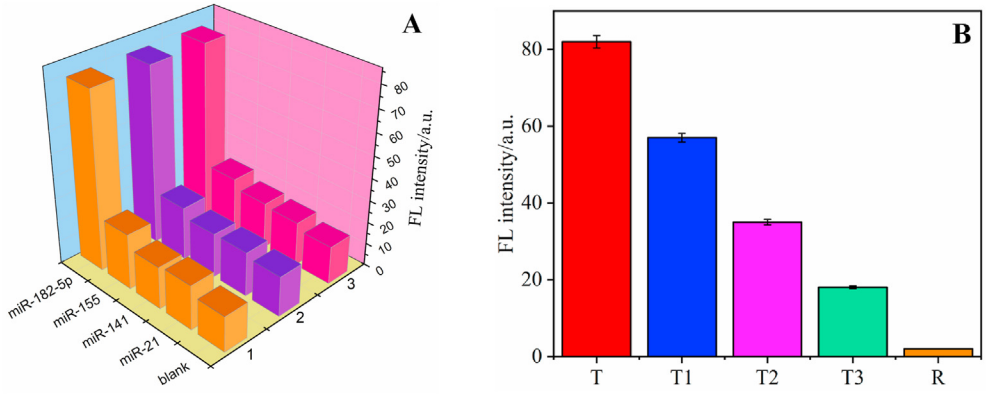

Fig. 8. (A) Specificity of the fluorescence biosensor for detecting different miRNAs, three sets of parallel experiments for 1 (orange), 2 (purple) and 3 (pink) columns. (B) Specificity of the fluorescence biosensor for different isomiRs of the target microRNA. Target microRNA (T), single-base mismatched target (T1), two-base mismatched target (T2), three-base mismatched target (T3), and random sequence (R).

obtained from target in complex sample matrix and those in ideal sample matrix at the same concentrations were compared. Obviously, the difference between the two sets of signals is very small, indicating that the method has good anti-interference ability and shows application potential for target detection in practical complex systems.

4. Conclusions

In this study, a novel fluorescence biosensing platform based on unique target cross-chain displacement circular amplification strategy coupled with distance-dependent light-induced electron transfer was designed for detection of MicroRNA. The platform has several advantages. 1) Firstly, the DNA cross structure is cleverly designed to protect the restriction sites, then the primers, polymerase, and nicking enzymes catalyzed DNA cross-based target cycling and strand displacement reaction amplification reactions. After target miRNA is amplified by cycling, a large number of products ssDNA (S1 and S2) are output, which can greatly amplified the target concentration and much improved the detection sensitivity. 2) Based on high affinity of Ag+ and base cytosine (C), single-stranded DNA sequences rich in cytosine (C) were used to synthesize fluorescent DNA/AgNCs probe, and single-stranded DNA sequences rich in guanine (G) were synthesized G-quadruplexes quencher, which were used as electron donors and acceptors in subsequent PET processes, respectively. The amplified products S1 and S2 can hybridize with the flexible COM1 and COM2, respectively, forming a rigid double-stranded DNA to suppress the corresponding quenching of the PET process, thus the fluorescence is restored. The ingenious design for the signal and quenching probes into a system can make the biosensing detection more simple and fast. 3) The amplified product based on miRNA-182-5p can specifically restore fluorescence, and the recovered fluorescence signal increases with increasing concentration, achieving much amplified and selective target detection. Therefore, the proposed fluorescence biosensor can be applied to the quantification of miRNA-182-5p. The sensing system has great potential for early clinical diagnosis of miRNAs-related diseases.

Declaration of competing interest

The authors declare that they have no known competing financial interests or personal relationships that could have appeared to influence the work reported in this paper.

Acknowledgements

This work was supported by the National Natural Science Foundation of China (No. 22076089).

Appendix A. Supplementary data

Supplementary data to this article can be found online at https://doi.org/10.1016/j.aca.2020.12.044.

References

[1] R. Clarke, J. Halsey, S. Lewington, E. Lonn, J. Armitage, J.E. Manson, Arch. Intern. Med. 170 (2010) 1622–1631.
[2] G.Q. Zhou, F. Han, Z.L. Shi, L. Yu, X.F. Li, C. Yu, C.L. Shen, Eur. Rev. Med. Pharmacol. Sci. 21 (2017) 3377–3383.
[3] A. Fatica, I. Bozzoni, Nat. Rev. Genet. 15 (2014) 7.
[4] T. Li, D. Li, J. Sha, P. Sun, Y. Huang, Biochem. Biophys. Res. Commun. 383 (2009) 280–285.
[5] X. Li, L. Wang, C. Li, Chem. Eur J. 21 (2015) 6817–6822.
[6] Y. Chang, Y. Zhuo, Y. Chai, R. Yuan, Anal. Chem. 89 (2017) 8266–8272.
[7] Q. Huang, K. Gumireddy, M. Schrier, C. le Sage, R. Nagel, S. Nair, A. Egan D, A. Li, G. Huang, A.J. Klein-Szanto, P.A. Gimotty, D. Katsaros, G. Coukos, L. Zhang, E. Puré, R. Agami, Nat. Cell Biol. 10 (2008) 202–210.
[8] H. Hirata, K. Ueno, V. Shahryari, G. Deng, Y. Tanaka, Z. Laura Tabatabai, Y. Hinoda, R. Dahiya, PloS One 8 (2013), e55502.
[9] J.J. Ge, C.L. Li, Y. Zhao, X.J. Yu, G.F. Jie, Chem. Commun. 55 (2019) 7350–7353.
[10] J.J. Ge, Y. Zhao, X.S. Gao, H.K. Li, G.F. Jie, Anal. Chem. 91 (2019) 14117–14124.
[11] P. Zhang, X. Wu, R. Yuan, Y. Chai, Anal. Chem. 87 (2015) 3202–3207.
[12] B. Yurke, A.J. Turberfield, A.P. Mills, F.C. Simmel, J.L. Neuman, Nature 406 (2000) 605.
[13] W. Zheng, Y. Di, Y. Liu, G. Huang, Y. Zheng, Y. Zhang, W. Fang, Clin. Biochem. 46 (2013) 1566–1571.
[14] K.A. Cissell, Y. Rahimi, S. Shrestha, E.A. Hunt, S.K. Deo, Anal. Chem. 80 (2008) 2319–2325.
[15] A. Chen, S. Ma, Y. Zhuo, Y. Chai, R. Yuan, Anal. Chem. 88 (2016) 3203–3210.
[16] C.L. Li, H.K. Li, J.J. Ge, G.F. Jie, Chem. Commun. 55 (2019) 3919–3922.
[17] L. Zhang, J. Zhu, S. Guo, L. Tao, L. Jing L, E. Wang, J. Am. Chem. Soc. 135 (2013) 2403–2406.
[18] X. Yang, L. Gan, L. Han, E. Wang, J. Wang, Angew. Chem. Int. Ed. 52 (2013) 2022–2026.
[19] C.M. Ritchie, K.R. Johnsen, J.R. Kiser, Y. Antoku, R.M. Dickson, J.T. Petty, J. Phys. Chem. C 111 (2007) 175–181.